AIP Advances

Frustration and relaxation of antiferromagnetic domains reversed by magneto-electric field cooling in a Pt/Co/Au/Cr_2O_3/Pt-stacked film

Cite as: AIP Advances **8**, 125313 (2018); https://doi.org/10.1063/1.5053136
Submitted: 21 August 2018 • Accepted: 27 November 2018 • Published Online: 06 December 2018

Yu Shiratsuchi, Shunsuke Watanabe, Shogo Yonemura, et al.

Frustration and relaxation of antiferromagnetic domains reversed by magneto-electric field cooling in a Pt/Co/Au/Cr_2O_3/Pt-stacked film

Yu Shiratsuchi,[1,a] Shunsuke Watanabe,[1] Shogo Yonemura,[2]
Tatsuo Shibata,[2] and Ryoichi Nakatani[1]
[1]*Department of Materials Science and Engineering, Graduate School of Engineering, Osaka University, Suita, Osaka 565-0871, Japan*
[2]*Advanced Technology Development Center, TDK Corporation, Chiba 272-0026, Japan*

(Received 21 August 2018; accepted 27 November 2018; published online 6 December 2018)

Using magnetic domain observations, we investigated the reversal process of the perpendicular exchange bias polarity resulting from the antiferromagnetic Cr_2O_3 domain reversal driven by magneto-electric field cooling (MEFC). The exchange bias polarity changed from negative to positive with increasing electric field during MEFC. The relevant change in the magnetic domain revealed the stochastic appearance of the reversed magnetic domains that exhibit the positive exchange bias. The local magnetization curves suggest that the antiferromagnetic domain state after MEFC was frustrated because of energy competition between the interfacial exchange coupling and the bulk magneto-electric effect. The frustrated nature of the magnetic domain structure is supported by the training effect of the exchange bias after MEFC.
https://doi.org/10.1063/1.5053136

INTRODUCTION

Antiferromagnetic (AFM) spintronics has attracted increasing interest because of its potential for use in applications such as ultra-high-density storage and for investigations in fundamental physics such as ultrafast spin dynamics in the terahertz regime.[1,2] A key technique of AFM spintronics is controlling AFM spins and/or AFM domains. Because AFM materials do not possess spontaneous magnetization and spin polarization, it is difficult to detect the AFM spin/domain directly. Recent studies have employed a compensated ferrimagnet as a quasi-AFM material. This approach has yielded some useful results, such as very fast magnetic domain wall velocity.[3]

Another approach using pure AFM materials is to utilize a magneto-electric (ME) effect that can induce finite magnetization by an electric field E. Cr_2O_3 is a prototypical ME AFM material,[4–6] and it has been reported that Cr_2O_3 exhibits ferroic features under a finite magnetic or electric field.[7] The ME effect of Cr_2O_3 is, however, a linear effect, that is, the ferroic feature cannot persist at zero field. In terms of engineering applications, the problem to be solved is how to compensate for the linear effect, in other words, how to detect the ferroic feature after removing the external fields. One solution is to use the exchange bias that is caused by the interfacial exchange coupling between the AFM and ferromagnetic (FM) layers.[8,9] To date, using the FM/Cr_2O_3 stacked system, e.g., Pt/Co/Au/Cr_2O_3/Pt-stacked film, the ME-controlled Cr_2O_3 domain state and detection via the exchange bias polarity have both been reported.[8–18] In this scenario, the ME-controlled AFM domain is implicitly supposed to be coupled with the FM domain.[13] However, direct results showing the relevant change in the magnetic domain structure with ME-induced switching of the exchange bias polarity has not yet been reported. This is mainly because direct observation of the AFM domain is

[a]Corresponding author. E-mail: shiratsuchi@mat.eng.osaka-u.ac.jp

quite difficult. Previously, X-ray magnetic linear dichroism (XMLD) successfully allowed observation of the AFM domain, for example, in Co/$LaFeO_3$ and Co/NiO where the in-plane component of AFM spins was visualized.[19,20] In contrast, for the perpendicular spin system suitable for modern spintronic devices, the AFM spin orientation is sometimes restricted to up or down, as with the FM/Cr_2O_3(0001) system. XMLD cannot distinguish such collinear spin structure. X-ray magnetic circular dichroism (XMCD) overcomes this limitation. Previously, we observed FM and interfacial AFM domains in a Pt/Co/Cr_2O_3/Pt-stacked film in an element-specific manner using a scanning XMCD microscope[21] and found that the FM and interfacial AFM magnetic domains were spatially coupled.[22] This finding means that the interfacial AFM domain can be imaged through the FM domain in this system. On the basis of this finding, in this study we have investigated the change in the magnetic domain pattern induced by ME-induced switching of the perpendicular exchange bias through the FM domain observation using a magneto-optic Kerr effect (MOKE) microscope.

EXPERIMENTAL

Pt(3.0)/Co(0.7)/Au(1.0)/Cr_2O_3(150)/Pt(20)-stacked film grown on an α-Al_2O_3(0001) substrate was used as the test sample. The numbers in parentheses are the thicknesses of the layers in nanometers. The film was prepared using a DC magnetron sputtering system with a base pressure below 5×10^{-7} Pa. The details of the film fabrication procedure, e.g., growth temperature, sputtering condition, etc., can be found in our previous paper.[23] Reflection high-energy electron diffraction observations (not shown) that were carried out in situ after depositing each layer revealed the growth of Pt(111) and Cr_2O_3(0001) beneath the Pt/Co/Au layer. The magnetization curve measured by means of a vibrating sample magnetometer showed that the film possessed perpendicular magnetic anisotropy. Based on MOKE magnetometry with a polar configuration, it was confirmed that the film exhibited a perpendicular exchange bias.

In this study, the MEFC technique was employed to switch the perpendicular exchange bias polarity.[8,10,11,17,18] In principle, MEFC should be started from above the Néel temperature of the Cr_2O_3 layer. For the FM/AFM stacked film, the Néel temperature can be estimated based on the temperature dependence of the exchange bias field H_{EX}.[24] As shown in Fig. 1, H_{EX} vanished at

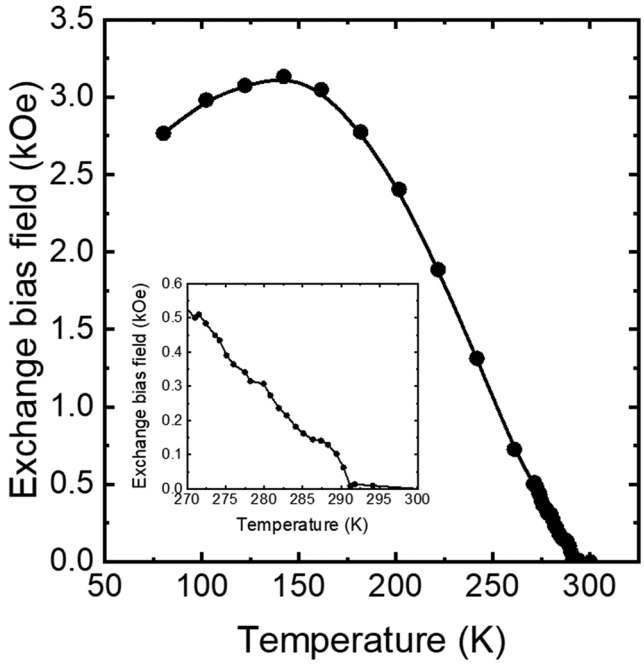

FIG. 1. Temperature dependence of the exchange bias field. Inset shows the enlarged figure in the vicinity of the Néel temperature.

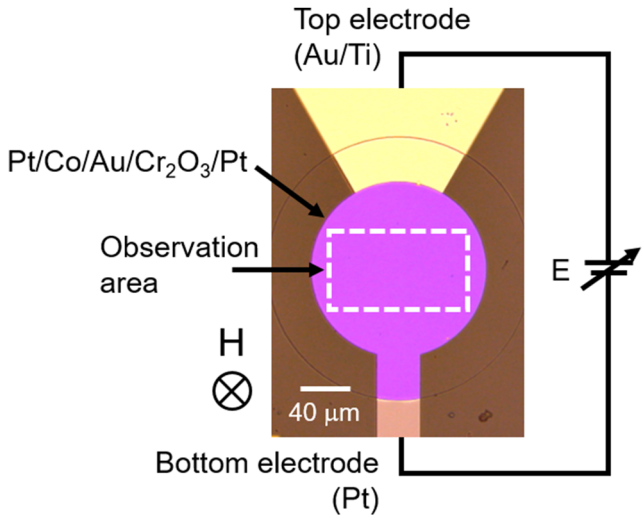

FIG. 2. Optical microscope image of the fabricated micro-dot with a diameter of 200 μm. The circuit diagram to apply the electric field is also shown. Magnetic domain observations by the MOKE microscope were made in the region shown by the white dotted line.

around 290 K, which we defined as the apparent Néel temperature. MEFC and the observation of the resultant magnetic domain were carried out using the following protocol.

(1) **Define the initial state by MEFC**. The film was cooled from 297 to 280 K at a rate of 4 K min^{-1}. Following cooling, a magnetic field H of +15 kOe and an electric field E were simultaneously applied.
(2) **Magnetic domain observation as a function of H**. After stabilizing the temperature at 280 K, E was switched off. At $E = 0$ kV cm^{-1}, the magnetic domain patterns were observed as a function of H with ±1.0 kOe. From the set of magnetic domain patterns, the H-dependence of the Kerr contrast could be obtained, equivalent to the magnetization curve within the observation area.

Processes (1) and (2) were repeated for various values of E, which was varied in the range 0 to +600 kV cm^{-1}. From the above measurements, the apparent exchange bias field H_{EX} and the apparent remanence ratio M_R/M_S were obtained as a function of E. The positive direction of the field is defined as the direction from the bottom electrode to the top electrode. It should be noted that the leakage current at +600 kV cm^{-1} was about 5×10^{-3} A cm^{-2}, sufficiently low to rule out a current-driven switching mechanism.

In order to apply E, the film was patterned into a micro-dot structure with a diameter of 200 μm using photolithography, Ar ion milling, and the lift-off process. The bottom 20 nm-thick Pt layer served as the bottom electrode to apply E to the Cr_2O_3 layer; the direction of E was perpendicular to the surface. An optical microscope image of the device with the equivalent circuit diagram to apply E is shown in Fig. 2. Using the fabricated micro-dot, magnetic domain observations by means of the MOKE microscope were carried out. The observed region is indicated by the dotted line in Fig. 2. The microscope was designed so that the magnetic domain with perpendicular magnetization was easily observable.

RESULTS AND DISCUSSION

Figure 3(a) shows the H-dependence of the Kerr contrast after MEFC with various E values. The Kerr contrast data were collected over the whole of the observed area. Below an E of 267 kV cm^{-1}, a fully negative exchange bias with $M_R/M_S = 1$ was observed. This is simply understood as the AFM domain state determined by the interfacial exchange coupling with FM magnetization. When E was increased to 333 kV cm^{-1}, the loop shape started to change; the remanent magnetization of the descending branch of the loop started to decrease while the apparent exchange bias

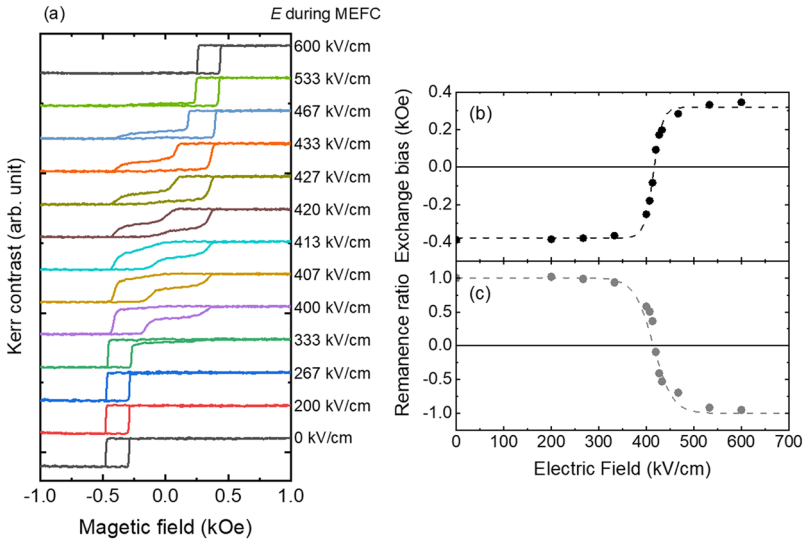

FIG. 3. (a) Magnetic-field dependence of the Kerr contrast, corresponding to the magnetization curve after MEFC under various E conditions. The Kerr contrast data were collected from the whole area of observation; (b) change in exchange bias field and (c) remanence ratio obtained from (a) with electric field during MEFC. The dotted lines in (b) and (c) represent the fitted curve using $\tanh(\Delta G/k_{\mathrm{B}}T)$.

remained unchanged. The changes in H_{EX} and $M_{\mathrm{R}}/M_{\mathrm{S}}$ became distinct above E = 400 kV cm^{-1}. At E = 420 kV cm^{-1}, the positive and negative exchange biases were almost balanced, and above E = 427 kV cm^{-1}, the positive exchange bias prevailed, and finally, at E = 600 kV cm^{-1}, the fully positive exchange-biased state was obtained. A similar change in the shape of the magnetization curve following MEFC has been reported previously.[18] In Figs. 3(b) and (c), the apparent H_{EX} and the apparent $M_{\mathrm{R}}/M_{\mathrm{S}}$ as a function of E are shown, respectively. The changes in H_{EX} and $M_{\mathrm{R}}/M_{\mathrm{S}}$ with E were gradual and could be reproduced by $\tanh(\Delta G/k_{\mathrm{B}}T)$, where k_{B} is the Boltzmann constant and T is the absolute temperature. ΔG represents the energy difference between the positive and negative exchange-biased states and can be expressed as[17,18]

$$\Delta G = \left[(\alpha E + M_{\mathrm{AFM}})H - \frac{J_{\mathrm{INT}}}{t_{\mathrm{AFM}}}\right]V_{\mathrm{AFM}} \tag{1}$$

where α is the ME coefficient (s m^{-1}), M_{AFM} is the uncompensated AFM moment in the Cr_2O_3 layer (Wb m^{-2}), J_{INT} is the interfacial exchange coupling energy (J m^{-2}), t_{AFM} is the AFM layer thickness (m), and V_{AFM} is the activation volume (m^3). The functional form of $\tanh(\Delta G/k_{\mathrm{B}}T)$ is derived from the switching probability and is dominated by the Boltzmann distribution of the oppositely directed domains. Some researchers have considered that finite magnetization in the Cr_2O_3 layer was induced by various defects[18,25] and contributed to M_{AFM}. In our case, the defect-induced finite magnetization is negligibly small and M_{AFM} is dominated by the interfacial uncompensated AFM moment.[16] In either case, from the changes in H_{EX} and $M_{\mathrm{R}}/M_{\mathrm{S}}$ with E for the various MEFC conditions, quantitative analysis may be possible, as previously carried out by Nozaki *et al.*[18] However, this is actually a nontrivial problem, as discussed below. Here, we simply note that the results shown in Figs. 3(a) and (b) could be reproduced by Eq. (1) as shown by the dotted lines. In the following discussion, we focus on the relevant change in the magnetic domain pattern after MEFC.

Figure 4 shows the magnetic domain pattern at the remanent state after MEFC in the transition regime, i.e., E = 400–433 kV cm^{-1}. With increasing E, the dark gray region increased. Comparing the images for E = 400–413 kV cm^{-1}, it is likely that the nucleation size of the reversed domain is about a few micrometers. While the total area of the reversed domain increased with increasing E, stochastic nucleation of the individual reversed domain occurred. For example, as indicated by the circles in Figs. 4(b) and (c), the nucleated domain at E = 407 kV cm^{-1} (solid yellow circle) was not observed at E = 413 kV cm^{-1} (broken yellow circle). This indicates that nucleation of the

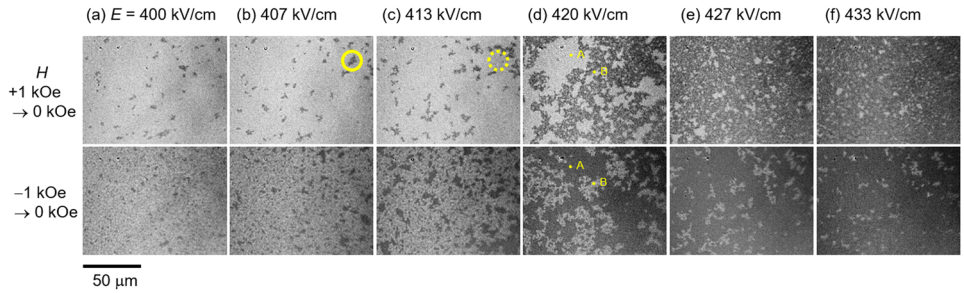

FIG. 4. Magnetic domain patterns at the remanent state. Top and bottom images show the magnetic domain at the remanent state in descending and ascending branches, respectively. Magnetic domain observations were made after MEFC with electric fields of: (a) 400, (b) 407, (c) 413, (d) 420, (e) 427, and (f) 433 kV cm^{-1}. Yellow circles represent the stochastic nucleation of the reversed domain (see text). A and B in (d) are the points at which the local magnetization (see text and Fig. 5) was collected.

reversed domain was thermally activated, confirming that the switching probability is expressed by $\tanh(\Delta G/k_{\mathrm{B}}T)$ as discussed above. Meanwhile, magnetic domain wall creep can also occur, as inferred from the shape of the magnetic domain wall that is similar to that observed in the creep regime for the $[\mathrm{Co/Pt}]_2$/Co/IrMn/Pt/Ta multilayer.[26]

Here, we discuss the magnetization reversal of the individual domain by means of the H-dependence of the Kerr contrast at the local points on the magnetic domain collected from the sequence of the magnetic domain image. Hereafter, the above curve is described as the local magnetization curve. In Fig. 5, the local magnetization curves measured on the magnetic domains labeled in Fig. 4(d) are shown. The Kerr contrast data were collected from a region of 10 × 10 pixels, or approximately 0.8 × 0.8 μm^2. The apparent exchange biases at positions A and B were positive and negative, respectively. However, the magnetization curves showed double-step switching in the descending (ascending) branch at position A (B), which was not observed in the ascending (descending) branch. This complex magnetization curve suggests that the magnetic domain state in the AFM layer is not uniform along the depth direction and is highly frustrated at the intermediate state, i.e., $E = 400$–433 kV cm^{-1}. The frustration of the ME-switched AFM domain was previously reported in $[\mathrm{Pd/Co}]_3$/Pd/$\mathrm{Cr_2O_3}$-subst. where the ME switching was induced in an isothermal manner in contrast to the MEFC.[27]

As previously reported,[22] the FM domain pattern should trace the interfacial AFM domain pattern. It is not, however, clear that the AFM domain state is uniform along the depth direction. In the phenomenological model,[17,18,27,28] the energy condition of MEFC-driven switching of the exchange bias is determined by the competition between the interfacial exchange coupling and the

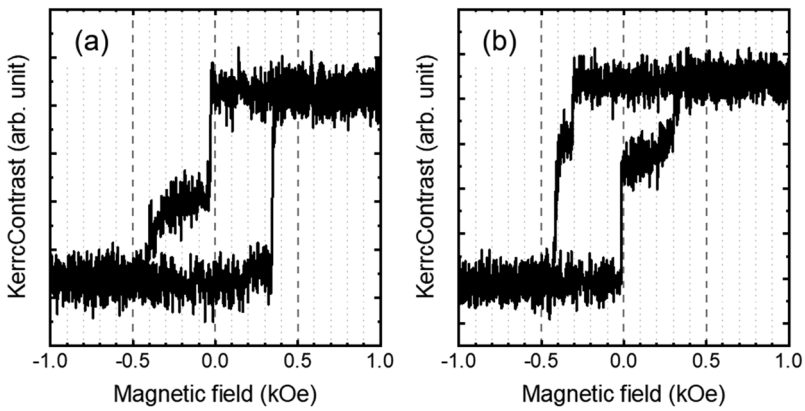

FIG. 5. Magnetic-field dependence of the Kerr contrast, corresponding to the local magnetization curve obtained at points (a) A and (b) B shown in Fig. 4(d), respectively.

ME effect; in our employed field direction, these two favor negative and positive exchange biases, respectively (see also Eq. (1)). Under such energy competition, a non-uniform frustrated AFM domain state was inferred at the intermediate state as reported by Echtenkamp and Binek.[27] Namely, at the intermediate state, the staggered magnetization of Cr_2O_3 reversed beneath the interface, whereas that near the interface remained because an excess energy barrier is required to reverse the staggered magnetization owing to the interfacial exchange coupling with the FM layer. In particular, when the interfacial exchange coupling between the Cr^{3+} and FM spins is stronger than that between the Cr^{3+}–Cr^{3+} spin pair in Cr_2O_3, the supposed complex AFM domain structure can be generated. A stronger interfacial exchange coupling than that at the bulk site has been predicted theoretically[29] and is to be expected from the experimental fact that XMCD from the interfacial Cr spin was detected above the apparent Néel temperature.[22]

When the complex domain structure is formed, the magnetic domain state should be frustrated within the Cr_2O_3 layer. The frustrated magnetic domain can rearrange by means of the magnetic field cycle into a more stable one. This is detectable as the training effect of the exchange bias.[27] As shown in Fig. 6, both M_R/M_S and the magnetic domain pattern at the remanent state change with the number of the magnetic field cycle N. The gray region increased overall with increasing N, whereas some gray regions vanished when N was low, i.e., $N \leq 3$. For $N > 3$, the changes in M_R/M_S and the magnetic domain pattern became more gradual, meaning that the magnetic domain structure was tending to be more stable. When the AFM layer has uniaxial magnetic anisotropy, as in the case of Cr_2O_3, rearrangement of the AFM spins within the individual domain does not occur.[30,31] That is, as long as the AFM layer is uniform along the depth direction, the training effect vanishes. In other words, the appearance of the training effect is relevant to the frustrated AFM

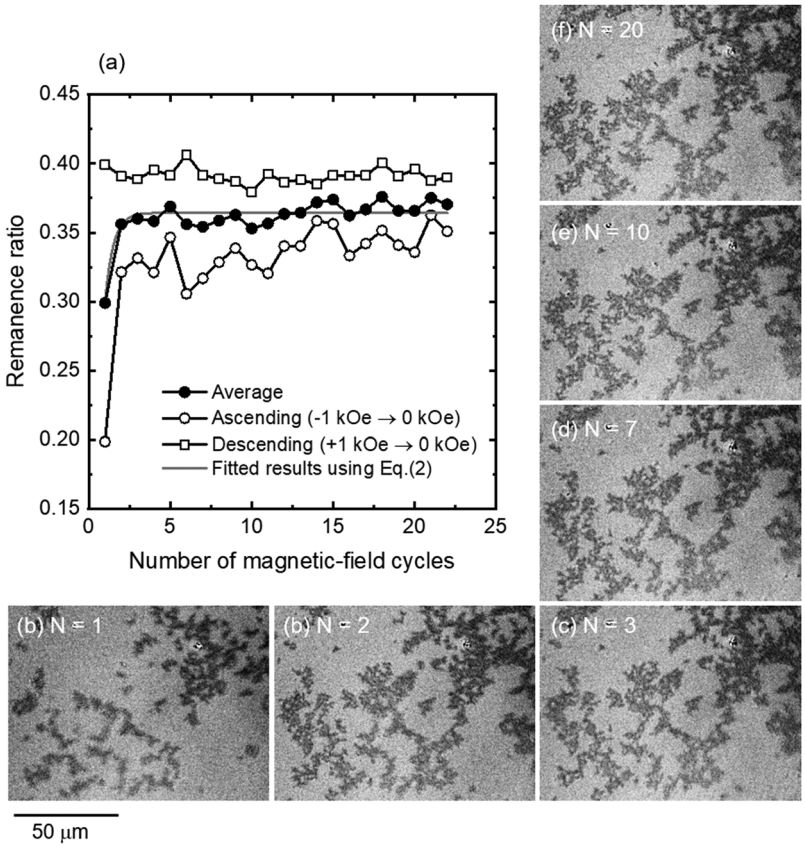

FIG. 6. (a) Changes in remanence ratio in descending (open circle) and ascending (open square) branches of the magnetization curve. Gray line represent the fitted results using Eq. (2). The closed circle represents the averaged value; (b)–(f) represent the magnetic domain pattern at the remanent state in the descending branch after the magnetic field cycle.

domain state after MEFC. The training effect of the exchange bias can be analyzed using the following equation.[27,32]

$$H_{EX}(N) = (K+1)^{N-1}\left\{H_{EX}(1) - KH_{EX}(\infty)\left[\frac{(K+1)^{N+1}}{K(K+1)^{N-1}} - (K+2)\right]\right\} \quad (2)$$

where K is constant to express the decay of the training and the intuitive meaning of K was discussed in Ref. 33. Here we use M_R/M_S as a parameter to represent the frustrated state as discussed above instead of $H_{EX}(N)$, and the application of Eq. (2) to Fig. 5(b) (shown by the solid gray line) yielded $K = -0.85 \pm 0.1$. Independently, the parameter-free $K(H_{EX}(E))$ can be expressed as[27]

$$K = -1 + 4\left(\frac{H_{EX}(E) - \frac{1}{2}\left(H_{EX}^{max} + H_{EX}^{min}\right)}{H_{EX}^{max} - H_{EX}^{min}}\right)^2 \quad (3)$$

Using $H_{EX}(E)$, $H_{EX}{}^{max}$ and $H_{EX}{}^{min}$ estimated from Fig. 3(b), K can be calculated as −0.90, roughly agrees with K estimated from Eq. (2) indicating the validity of the above mechanism.

The similar frustration of the AFM domain state and the resultant training effect of the exchange bias at the intermediate state was previously found in $[Pd/Co]_3/Pd/Cr_2O_3$-subs.[27] In the previous report, the isothermal switching using the Cr_2O_3 single crystal substrate was adopted whereas we adopted the MEFC-driven switching using the Cr_2O_3 thin film in this work. The fact that the frustrated AFM domain was observed for the different switching mode implies that the frustration of the AFM domain is common for the ME-induced switching. Besides, in these two cases, the Cr_2O_3 thickness is highly different: typically 0.5 mm for the former case and 150 nm for our case, implying that the frustration of the AFM domain state occurred in the vicinity of the interface, consistent with the above supposed mechanism to generate the frustration of the AFM domain state.

To verify that this frustrated AFM domain state was the result of MEFC, i.e., the above-mentioned energy competition, we further investigated the magnetization curves and the training effect after conventional zero-field cooling (ZFC). The film was demagnetized at 298 K by the magnetic field cycle and cooled to 280 K, keeping the demagnetized state. Figures 7(a) and (b) show the magnetization curve from the whole area and those on the bright and dark areas. In contrast to Fig. 3(a), the magnetization curve of the whole area exhibited two-step magnetization reversal in both descending and ascending branches, indicating the co-existence of positive and negative exchange-biased states. In addition, the magnetization curves on the bright and dark areas show simple magnetization reversal exhibiting positive and negative exchange biases, respectively. Furthermore, as shown in Fig. 7(c), the training effect was not observed. In the case of conventional cooling, the AFM domain state

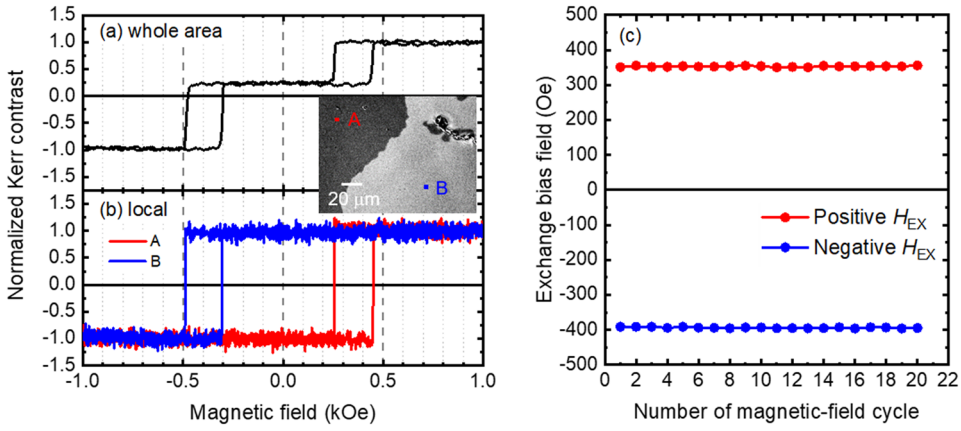

FIG. 7. Magnetic-field dependence of the Kerr contrast collected from (a) whole observed area and (b) at local points after zero-field cooling in keeping the multi-domain state. Points A and B at which the local magnetization curves were collected are shown in the inset, the magnetic domain pattern at the remanent state; (c) changes in the positive (red) and negative (blue) exchange bias fields with magnetic field cycle.

was determined by the interfacial exchange coupling with the FM spins, and the above-mentioned energy competition does not occur. Consequently, the AFM domain should be simple along the depth direction.

The previously derived model for MEFC-driven switching simply assumed two types of domains possessing positive and negative exchange biases, and the distribution of the staggered magnetization along the depth direction was not taken into consideration. Consequently, the probability distribution of the two domains proportional to the Boltzmann distribution yielded the above-mentioned E-dependence of H_{EX} (and M_R/M_S), $\propto \tanh(\Delta G/k_B T)$. However, this simple assumption is obviously invalid in explaining the above local magnetization curve and the training effect. For a more precise understanding of the energy condition of MEFC-driven switching, a deeper understanding of the magnetic domain state is essential.

SUMMARY

We have investigated the change in the magnetic domain pattern accompanying switching of the perpendicular exchange bias driven by MEFC. Both the apparent H_{EX} and the apparent M_R/M_S changed with E during MEFC, in agreement with the results of previous studies. Nucleation of the reversed domain exhibiting positive exchange bias was stochastically observed, suggesting that thermal activation played a significant role. The local magnetization curve exhibited the complex magnetization process, which suggested that the AFM domain state in the vicinity of the interface is different from that beneath the interface. The complex AFM domain state yields the frustrated AFM domain state, which results in the training effect that was not observed following the conventional ZFC process.

ACKNOWLEDGMENTS

This work was partly supported by JSPS KAKENHI (Grant Nos. 16H03832 and 16H02389) and by the Photonics Advanced Research Center (PARC) at Osaka University.

[1] V. Baltz, A. Manchon, M. Tsoi, T. Moriyama, T. Ono, and Y. Tserkovyak, Rev. Mod. Phys. **90**, 015005 (2018).
[2] M. B. Jungfleish, W. Zhang, and A. Hoffmann, Phys. Lett. A **382**, 865 (2018).
[3] K. Kim, S. K. Kin, Y. Hirata, S.-H. Oh, T. Tono, D.-H. Kim, T. Okuno, S. Ham, S. Kim, G. Go, Y. Tserkovyak, A. Tsukamoto, T. Moriyama, K.-J. Lee, and T. Ono, Nature Mater. **16**, 1187 (2017).
[4] D. N. Astrov, Sov. Phys. JETP **11**, 708 (1960).
[5] V. J. Folen, G. T. Rado, and E. W. Stadler, Phys. Rev. Lett. **6**, 607 (1961).
[6] T. H. O'Dell, *The Electrodynamics of Magneto-electric Media* (North-Holland Publishing Company, 1970).
[7] A. Iyama and T. Kimura, Phys. Rev. B **87**, 180408(R) (2013).
[8] P. Borisov, A. Hochstrat, X. Chen, W. Kleemann, and C. Binek, Phys. Rev. Lett. **94**, 117203 (2005).
[9] X. He, Y. Wang, A. N. Caruso, E. Vosocovo, K. D. Belashchenko, P. A. Dowben, and C. Binek, Nature Mater. **9**, 579 (2010).
[10] K. Toyoki, Y. Shiratsuchi, T. Nakamura, C. Mitsumata, S. Harimoto, Y. Takechi, T. Nishimura, H. Nomura, and R. Nakatani, Appl. Phys. Express **7**, 114201 (2014).
[11] T. Ashida, M. Oida, N. Shimomura, T. Nozaki, T. Shibata, and M. Sahashi, Appl. Phys. Lett. **104**, 152409 (2014).
[12] T. Ashida, M. Oida, N. Shimomura, T. Nozaki, T. Shibata, and M. Sahashi, Appl. Phys. Lett. **106**, 132407 (2015).
[13] K. Toyoki, Y. Shiratsuchi, A. Kobane, C. Mitsumata, Y. Kotani, T. Nakamura, and R. Nakatani, Appl. Phys. Lett. **106**, 162404 (2015).
[14] K. Toyoki, Y. Shiratsuchi, A. Kobane, S. Harimoto, S. Onoue, H. Nomura, and R. Nakatani, J. Appl. Phys. **117**, 17D902 (2015).
[15] T. V. A. Nguyen, Y. Shiratsuchi, and R. Nakatani, Appl. Phys. Express **10**, 083002 (2017).
[16] T. V. A. Nguyen, Y. Shiratsuchi, A. Kobane, S. Yoshida, and R. Nakatani, J. Appl. Phys. **122**, 073905 (2017).
[17] M. Al-Mahdawi, S. P. Pati, Y. Shiokawa, S. Ye, T. Nozaki, and M. Sahashi, Phys. Rev. B **95**, 144423 (2017).
[18] T. Nozaki, M. Al-Mahdawi, S. P. Pati, S. Ye, Y. Shiokawa, and M. Sahashi, Jpn. J. Appl. Phys. **56**, 070302 (2017).
[19] F. Nolting, A. Scholl, J. Stöhr, J. W. Seo, J. Fompeyrine, H. Seigwark, J.-P. Locquiet, S. Anders, J. Lüning, E. E. Fullerton, M. F. Toney, M. R. Schenfein, and H. A. Padmore, Nature **405**, 767 (2000).
[20] L. Duó, M. Finazzi, and F. Ciccacci, *Magnetic Properties of Antiferromagnetic Oxide Materials* (Wiley-VCH Verlag GmBH & Co. KGaA, 2010), pp. 301–339.
[21] Y. Kotani, Y. Senba, K. Toyoki, D. Billington, H. Okazaki, A. Yasui, W. Ueno, H. Ohashi, S. Hirosawa, Y. Shiratsuchi, and T. Nakamura, J. Synchrotron Rad. **25**, 1444 (2018).
[22] Y. Shiratsuchi, Y. Kotani, S. Yoshida, Y. Yoshikawa, K. Toyoki, A. Kobane, R. Nakatani, and T. Nakamura, AIMS Mater. Sci. **2**, 484 (2015).
[23] Y. Shiratsuchi, W. Kuroda, T. V. A. Nguyen, Y. Kotani, K. Toyoki, T. Nakamura, M. Suzuki, K. Nakamura, and R. Nakatani, J. Appl. Phys. **121**, 073902 (2017).

[24] D. Lederman, J. Nogués, and I. K. Schuller, Phys. Rev. B **56**, 2332 (1997).
[25] T. Kosub, M. Kopte, R. Hühne, P. Appel, B. Shields, P. Maletinsky, R. Hübner, M. O. Liedke, J. Fassbender, O. G. Schmidt, and D. Makarov, Nat. Comm. **8**, 13985 (2017).
[26] Q. Wu, W. He, H.-L. Liu, Y.-F. Liu, J.-W. Cai, and Z.-H. Cheng, J. Appl. Phys. **113**, 033901 (2013).
[27] W. Echtenkamp and Ch. Binek, Phys. Rev. Lett. **111**, 187204 (2013).
[28] Y. Shiratsuchi and R. Nakatani, Mater. Trans. **57**, 781 (2016).
[29] R. Choudary, T. Komesu, P. Kumar, P. Manchandra, K. Taguchi, T. Okuda, K. Miyamoto, P. A. Dowben, R. Skomski, and A. Kashyap, EPL **115**, 17002 (2016).
[30] A. Hoffmann, Phys. Rev. Lett. **93**, 097203 (2004).
[31] K. D. Balashchenko, Phys. Rev. Lett. **105**, 147204 (2010).
[32] Ch. Binek, S. Polisetty, X. He, and A. Berger, Phys. Rev. Lett. **96**, 067201 (2006).
[33] S. Polisetty, S. Sahoo, A. Berger, and Ch. Binek, Phys. Rev. B **78**, 184426 (2008).